Evaluation of CMIP5 and CMIP6 Models Based on Weather Types Applied to the South Atlantic Ocean

Luana Borato[1], Antonio Fernando Härter Fetter Filho[1], Paula Gomes da Silva[1,2], Fernando Javier Mendez[3], Antonio Henrique da Fontoura Klein[1]

Affiliations

1. Special Oceanography Coordination, Federal University of Santa Catarina, Florianópolis, SC, 88040-900, Brazil

2. Environmental Hydraulics Institute "IH Cantabria", University of Cantabria, Scientific and Technological Park of Cantabria, Santander, Spain

3. Department of Sciences and Techniques in Water and Environment, University of Cantabria, Santander, Spain

Corresponding author(s): Luana Borato (boratoluana@gmail.com)

Abstract

Changes in climate in the South Atlantic region and adjacent regions have been described in numerous works using projections from global climate models from CMIP5 and CMIP6. This paper presents an evaluation of the ability of these models to reproduce the atmospheric circulation patterns (weather types) and their seasonal and inter-annual variability. The analyzes are performed based on the probability of occurrence of weather types in the historical period and in future projections. The scatter index and the relative entropy are the statistical parameters used to evaluate the models' performance in the historical period. Future projections consist of RCP2.6, 4.5 and 8.5 scenarios for the CMIP5 models and the SSP126, 245, 370 and 585 scenarios for the CMIP6 and are assessed at different time intervals: short term (2015-2039), mid-term (2040-2069) and long term (2070-2100). The performance of projections is measured by analyzing their consistency, that is, based on the similarity between projections of the same scenario in different models. The results show that the reproduction of the probability of occurrence of historical weather types and their seasonal and interannual variability was better performed by ACCESS1-0, HadGEM2-ES, HadGEM2-CC, CMCC-CM and MPI-ESM-P when assessing the models from CMIP5, and by HadGEM3-GC31-MM, ACCESS-ESM1-5, ACCESS- CM2 and MRI-ESM-P when assessing the models from CMIP6. As for future projections, only the BESM-AO2-5, GFDL-ESM4 and HadGEM3-GC31-MM models showed inconsistency in one or more scenarios.

Keywords: Global Climate Models. Climate Change. South Atlantic, performance assessment.

1. Introduction

The outputs of global climate models (GCMs) are essential to support and understand climate changes around the world (Swart & Fyfe, 2012; Fant et al., 2016; Cherchi et al., 2018, Cagigal et al., 2020; Kreienkamp et al., 2020; Berg & McColl, 2021). Since the early 1990s, the World Climate Research Program (WCRP) has coordinated the Coupled Models Intercomparison Project (CMIP) to promote common simulations with different GCMs to better understand the climate variability in the past, present, and future (Meehl et al., 1997; Meehl et al., 2005; Bock et al., 2020; Touzé-Peiffer et al., 2020). GCMs outputs are commonly used as input in dynamic and statistical downscaling experiments, in order to generate secondary information such as wave, storm surge, river discharge and precipitation data (Fowler et al., 2007; Camus et al., 2017; Perez et al., 2015).

Several studies show the applicability and performance of GCMs in different regions of the world (Reichler & Kim., 2008; Hall et al., 2019; Fasullo, 2020; Fasullo et al., 2020). One of the methods applied to evaluate the performance of GCMs relies on the assessment of their capability to reproduce the atmospheric circulation patterns (i.e., weather types) (Huth, 2000; Pastor & Casado, 2012; Perez et al., 2014; Abadi et al., 2018, Olmo et al., 2023). The results from these analyses are particularly important to understand how GCMs performs when representing weather types, and have great value for studies that relate weather type patterns, the resultant oceanographic condition and the effect of climate change on it.

In the North Atlantic, analyses of GCMs in terms of their ability to reproduce the probability of weather types have been widely explored (e.g. Perez et al., 2014; Camus et al., 2014). However, although GCMs are commonly used to support climate change studies in the South Atlantic (Vera et al., 2006; He et al., 2017; Reboita et al., 2018; Villamayor et al., 2018), little is known regarding their performance on reproducing the atmospheric patterns in this region (Hofstadter & Bidegain, 1997; Bidegain, 2006; Yin et al., 2013; Abadi et al., 2018, Reboita et al., 2019).

This paper presents a performance assessment of GCMs in the South Atlantic through the methodology described by Perez et al. (2014). The methodology consists of analyzing the skill of GCMs when reproducing the historical probability of occurrence of weather types, as well as, evaluating the consistency of their future projections. The weather types applied here were obtained during the project Regional Oceanographic and Amospheric Downscaling (ROAD https://road-besm.ufsc.br/) in which daily sea level pressure (SLP) fields and sea level pressure gradient (SLPG) were used as input in a classification analysis to define the typical weather types that occur over the Southeast coast of the Atlantic Ocean. The SLP fields contain surface climate conditions and has been shown to be a good predictor for waves, storm surge and total water level (Cagigal et al., 2020; Camus et al., 2014; Rueda et al., 2016). Here, statistical metrics (scatter index and relative entropy) are estimated to evaluate the performance of 48 GCMs, 27 from

CMIP5 (Taylor et al., 2012) and 21 from CMIP6 (Eyring et al., 2016) on reproducing the probability of occurrence of the historical weather types (Table 1). The consistency of future projections of RCPs (Representative Concentration Pathways - van Vuuren et al., 2011) and SSPs (Shared Socioeconomic Pathways - O'Neill et al., 2017) scenarios and the magnitude of changes in the probability of occurrence of each weather type were also evaluated.

2. Study area, data and methods

2.1. Study area

This study investigates the regional atmospheric circulation patterns over the South Atlantic Ocean, with a particular focus on the southeastern Brazilian coast. The spatial limits of the study are within 0° and 70°S of latitude and 70°W and 20°E of longitude (Figure 1).

The climate over the South Atlantic and adjacent regions is dominated by the South Atlantic Subtropical Anticyclone (SASA). This system is defined by a semi-permanent subtropical high pressure with greater amplitude and intensity during the winter months (Peterson & Stramma, 1991; Degola, 2013; Sun et al., 2017; Reboita et al., 2019).

SASA is closely related to the wave climate of the Southern coast of Brazil, as it is responsible for the northeasterly winds that act over the ocean in the region (Degola, 2013). Wave conditions in this zone have shown to be also related to the passage of cold fronts (~10% of the occurrences), to the occurrence of semi-stationary (nearly-stationary) anticyclones that migrate to the north, resulting in waves from the east and southeast (~50% of the occurrences) and to non-local wind conditions that results in long-period waves that travel towards the study area (~30% of occurrences) (Alves & Melo, 2001). The occurrence of extreme wave events is mainly associated with cyclones generated between 30°S and 35°S and are intensified when they occur concomitantly with other atmospheric systems, such as extratropical transient anticyclones, resulting in persistent southwesterly winds, which are considered the main generators of extreme events in the region (Araújo et al., 2003; Gomes da Silva et al., 2016; Reboita et al., 2019; Gramcianinov et al., 2020).

The storm surge in this area is associated with the occurrence of frontal systems and with the evolution and persistence of low-pressure systems acting over the ocean, which lead to strong winds from southwest blowing parallel to the coast (Parise et al., 2009). Storm surge events are intensified when the cyclone occurs simultaneously with high pressure over the continent, which results in an increase in pressure gradient and, consequently, wind speed. Following Ekman theory, these strong winds rotate to east resulting in a wind setup, while the pressure gradient caused by the low pressure over the ocean increases the water level at the coast. Extreme values are typically observed during the austral winter and autumn, when the south wind speed is more

intense (Campos et al., 2010). The particular characteristic of this zone is the shallow shelf that takes the storm surge generated far South to propagate northward as a continental shelf wave and, as a result, the remote component dominates the storm surge signal at the coast (Melo, 2016).

2.2. *Data*

The weather types considered in this work were obtained during the development of the project ROAD. In that project weather types were obtained to be used as atmospheric predictor for wave and storm surge data at Florianópolis (South Brazil). In this paper, these weather types are used to analyze the skill of the CMIP5 and CMIP6 models to reproduce the main patterns of atmospheric circulation over the South Atlantic Ocean. The dataset used to obtain the weather types and to evaluate the performance of GCMs models are described in this section.

2.2.1. Reanalysis data

The historical weather types were computed using daily average fields of SLP from the Climate Forecast System Reanalysis (CFSR, Saha et al., 2010) (1979-2010). The spatial resolution used was 2° x 2°. Although, the original resolution of the CFSR fields is 1/4°, a sensitivity test have shown that the increase in spatial resolution did not affect the computed weather types.

2.2.2. Global Climate Models

The atmospheric data from the CMIP5 and CMIP6 (Taylor et al., 2012; Eyring et al., 2016) are used. The data consists of daily sea level pressure fields mapped onto a 2° x 2° spatial resolution grid, aligned with the grid of the reanalysis data. The collection of operators of the Climate Data Operator (CDO) was used for all data processing (Schulzweida, 2019).

Twenty-seven (27) models from CMIP5 and twenty-one (21) from CMIP6 are considered in the analyses (Table 1). Simulations for the historical period consider the period from 1979 to 2004. To ensure greater security in the comparison of models, the ensemble used were r1i1p1 for CMIP5 models and r1i1p1f1 for CMIP6 models. The scenarios analyzed here are RCP 2.6, RCP 4.5, and RCP 8.5 for CMIP5 and SSP126, SSP245, SSP370, and SSP585 for CMIP6. The analyzed scenarios for each GCM and for each time interval are indicated in Table 1. It is noteworthy that not all GCMs presented projections for all scenarios. In total, one hundred and twenty-two (122) future projections were analyzed. This number includes the separation of projected data by by scenarios and time interval (short, mid and long-term).

Table 1 – CMIP5 and CMIP6 Global Climate Models (GCMs) used in the analyses. Note that not all models had versions in both phases of CMIP or all scenarios considered. References from all GCMs are included in the manuscript reference list.

Model	Version	Atmospheric model	Atmospheric resolution (EWxNS)	CMIP5	CMIP6	Scenarios	Institute	Country	Reference
ACCESS	1-0	AGCM v1-0	1.875°x1.25°	x		RCP 4.5, 8.5	Bureau of Meteorology (Bureau) and Commonwealth Scientific and Industrial Research Organisation (CSIRO)	Australia	BI *et al.*. (2013)
	1-3	AGCM v1-0	1.875°x1.25°	x		RCP 4.5, 8.5			
	CM2	MetUM-HadGEM3-GA7.1	N96L85 (192 x 144 lon/lat)		x	SSP 126, 245, 370, 585			BI *et al.*. (2020)
	ESM1-5	HadGAM2	192 x 145 (lon/lat)		x	SSP 126, 245, 370, 585			ZIEHN *et al.*. (2020)
BESM	OA2-5	CPTEC/INP AGCM	1.875°x1.875° (T62L28)	x		RCP 4.5	National Institute for Space Research	Brazil	NOBRE *et al.* (2013)
CanESM	2	CanAM4 (AGCM15i)	T63L35	x		RCP 2.6, 4.5, 8.5	Canadian Centre for Climate Modelling and Analysis	Canada	ARORA *et al.* (2011)
	5	CanAM5	T63L49 (128 x 64 lon/lat)		x	SSP 126, 245, 370, 585			SWART *et al.* (2019)

Model	Version	Atmospheric model	Atmospheric resolution (EWxNS)	CMIP5	CMIP6	Scenarios	Institute	Country	Reference
CMCC	CESM	ECHAM5	T31L39 (96 x 48 lon/lat)	x		RCP 8.5	Centro EuroMediterraneo per I Cambiamenti Climatici	Italy	FOGLI *et al.* (2009)
	CM	ECHAM5	0.75°x 0.75°	x		RCP 4.5, 8.5			SCOCCIMARRO *et al.* (2011)
	CMS	ECHAM5	T63L95	x		RCP 4.5, 8.5			DAVINI *et al.* (2014)
CNRM	CM5	ARPEGE-Climat (V5.2.1)	TL127L31	x		RCP 2.6, 4.5, 8.5	Center National Weather Research	France	VOLDOIRE *et al.* (2013)
CESM	2	CAM6	0.9°x1.25° (288 x 192 lon/lat)		x	SSP 126, 245, 370, 585	Community Earth System Model Contributors	EUA	DANABASOGLU *et al.* (2020)
EC-Earth	3	IFS cy36r4	TL255 (512 x 256 lon/lat)		x	SSP 126, 245, 370, 585	EC -EARTH consortium	European group	MASSONNET *et al.* (2020); WYSER *et al.* (2020)
	3-Veg	IFS cy36r4	TL255 (512 x 256 lon/lat)		x	SSP 126, 245, 370, 585			
FGOALS	f3-L	FAMIL2.2	360 x 180 (lon/lat)		x	none	Institute of Atmospheric Physics (LASG) and Centre for Earth System Science (CESS)	China	HE *et al.* (2020)
	g3	GAMIL2	180 x 90 (lon/lat)		x	SSP 126, 245, 370, 585			LI *et al.* (2020)

140

Model	Version	Atmospheric model	Atmospheric resolution (EWxNS)	CMIP5	CMIP6	Scenarios	Institute	Country	Reference
GFDL	CM3	AM3p9	C48L48	x		RCP 2.6, 4.5, 8.5	Geophysical Fluid Dynamics Laboratory (NOAA)	EUA	DONNER *et al.* (2011)
	ESM2G	AM2p14	M45L24	x		RCP 2.6, 4.5, 8.5			DUNNE *et al.* (2012)
	ESM2M	AM2p14	M45L24	x		RCP 2.6, 4.5, 8.5			
	CM4	GFDL-AM4.0.1	360 x 180 (lon/lat)		x	SSP 245, 585			HELD *et al.* (2019)
	ESM4	GFDL-AM4.1	360 x 180 (lon/lat)		x	SSP 126, 245, 370, 585			DUNNE *et al.* (2020)
HadGEM	HadCM3	HadAM3	N48L19	x		none	Hadley Centre for Climate Prediction and Research	United Kingdom	GORDON *et al.* (2000)
	2-AO	HadGAM2	N96L38	x		RCP 2.6, 4.5, 8.5			COLLINS *et al.* (2011)
	2-CC	HadGAM2	N96L60	x		RCP 4.5, 8.5			
	2-ES	HadGAM2	L38N96L38 (1.25° × 1.875°)	x		RCP 2.6, 4.5, 8.5			
	3-GC31-HM	MetUM-HadGEM3-GA7.1	N512L85 (1024 x 768 lon/lat)		x	none			ANDREWS *et al.* (2019)
	3-GC31-LL	MetUM-HadGEM3-GA7.1	N96L85 (192 x 144 lon/lat)		x	SSP 126, 245, 585			

Model	Version	Atmospheric model	Atmospheric resolution (EWxNS)	CMIP5	CMIP6	Scenarios	Institute	Country	Reference
HadGEM	3-GC31-MM	MetUM-HadGEM3-GA7.1	N216L85 (432 x 324 lon/lat)		x	SSP 126, 585			ANDREWS *et al.* (2019)
INMCM	4		1.5° x 2°	x		RCP 4.5, 8.5	Institute for Numerical Mathematics	Russia	VOLODIN *et al.* (2010)
	4-8	INM-AM4-8	2°x1.5° (180 x 120 lon/lat)		x	SSP 126, 245, 370, 585			VOLODION *et al.* (2018)
	5-0	INM-AM5-0	2°x1.5° (180 x 120 lon/lat)		x	SSP 126, 245, 370, 585			VOLODIN *et al.* (2017a); VOLODIN *et al.* (2017b)
IPSL	CM5A-LR	LMDZ5_NPv3.1	96x95 (lon/lat)	x		RCP 2.6, 4.5, 8.5	Institut Pierre -Simon Laplace	France	DUFRESNE *et al.* (2013); MIGNOT *et al.* (2013)
	CM5A-MR	LMDZ4_v5	144x143 (lon/lat)	x		RCP 2.6, 4.5, 8.5			
	CM6A-LR	NPv6	N96L79 (144 x 143 lon/lat)		x	SSP 126, 245, 370, 585			BOUCHER *et al.* (2020)

Model	Version	Atmospheric model	Atmospheric resolution (EWxNS)	CMIP5	CMIP6	Scenarios	Institute	Country	Reference
MIROC	4h	AGCM5.8	T213L56	x		none	Atmosphere and Ocean Research Institute (The University of Tokyo), National Institute for Environmental Studies, and Japan Agency for marine - Earth Science and Technology	Japan	SAKAMOTO *et al.* (2012)
	5	MIROC-AGCM6	T85L40	x		RCP 2.6, 4.5, 8.5			WATANABE *et al.* (2010)
	ESM	MIROC-AGCM 2010	T42L80	x		RCP 2.6, 4.5, 8.5			WATANABE *et al.* (2011)
	ESM-CHEM	MIROC-AGCM 2010	T42L80	x		RCP 2.6, 4.5, 8.5			
	6	CCSR AGCM	T85L81 (256 x 128 lon/lat)		x	SSP 126, 245, 370, 585			TATEBE *et al.* (2019)
MPI-ESM	LR	ECHAM6	T63L47	x		RCP 2.6, 4.5, 8.5	Max Planck Institute für Meteorologie	Germany	GIORGETTA *et al.* (2013)
	MR	ECHAM6	T63L47	x		RCP 2.6, 4.5, 8.5			
	P	ECHAM6	T63L47	x		none			
	1-2-HAM	ECHAM6.3	T63L47 (192 x 96 lon/lat)		x	none			MAURITSEN *et al.* (2019); MÜLLER *et al.* (2018)
	1-2-HR	ECHAM6.3	T127L95 (384 x 192 lon/lat)		x	SSP 126, 245, 370, 585			
	1-2-LR	ECHAM6.3	T63L47 (192 x 96 lon/lat)		x	SSP 126, 245, 370, 585			

147

Model	Version	Atmospheric model	Atmospheric resolution (EWxNS)	CMIP5	CMIP6	Scenarios	Institute	Country	Reference
MRI	CGCM3	GSMUV-110112	TL159L48	x		RCP 2.6, 4.5, 8.5	Meteorological Research Institute	Japan	YUKIMOTO *et al.* (2012)
	ESM1	GSMUV-110120oc	TL159L48	x		RCP 8.5			YUKIMOTO *et al.* (2011)
	ESM2-0	MRI-AGCM3.5	TL159 (320 x 160 lon/lat)		x	SSP 126, 245, 370, 585			YUKIMOTO *et al.* (2019)

148

2.2.3. Wave data

Wave data were considered in the process of computing the weather types (more details in section 2.3). Wave parameters applied in the analyses were those from the hindcast model developed by the Australian Bureau of Meteorology and the Climate Science Center (CSIRO) (Durrant et al., 2014; Smith et al., 2021). Such database was generated using the WaveWatch III model (v4.08) forced with winds from NCEP CFSR (Saha et al., 2010) and daily sea ice. This hindcast provides bulk and partitioned wave parameters at a global resolution of 0.4° and spam from 1979 to 2010.

2.3. Methods

2.3.1. Computation of weather types

The methodology to compute the weather types as predictors for wave data within the project ROAD was the same applied by Rueda et al. (2016). It consists on i) calculating daily averaged atmospheric data (SLP and SLPG); ii) modifying the atmospheric data according to information about wave and storm surge propagation in the area of interest; iii) applying Principal Component Analysis (PCA) to reduce the dimensionality of the data and iv) applying a classification method that allows to group the atmospheric conditions in classes of weather types with similar characteristics. Some details of this process are presented in the following text.

The weather types were generated to be later related to nearshore waves. In that case, it was important to use the atmospheric data that actually generates the waves that reaches the coast of the study area. The waves observed in South Brazil are generated over the South Atlantic Ocean and travel for a few days before reaching the coast (Araújo et al., 2003; Truccolo, Franco, Schettini, 2004; Gomes da Silva et al., 2016; Melo, 2016). Wave propagation times over South Atlantic were obtained applying the ESTELA method (Perez et al., 2014b). ESTELA (a method for Evaluating the Source and Travel-time of the wave Energy reaching a Local Area) applies fields of wave spectra to estimate the effective energy flux (energy of the spectrum travelling towards the target point) based on the characteristics of the spectrum and the location of the source and target point. Finally, the travel time is obtained using a weighted mean of the group celerity. Figure 1 shows the isochrones that represent the propagation times of the waves (blue contours) that reach a target point in the Brazilian coast.

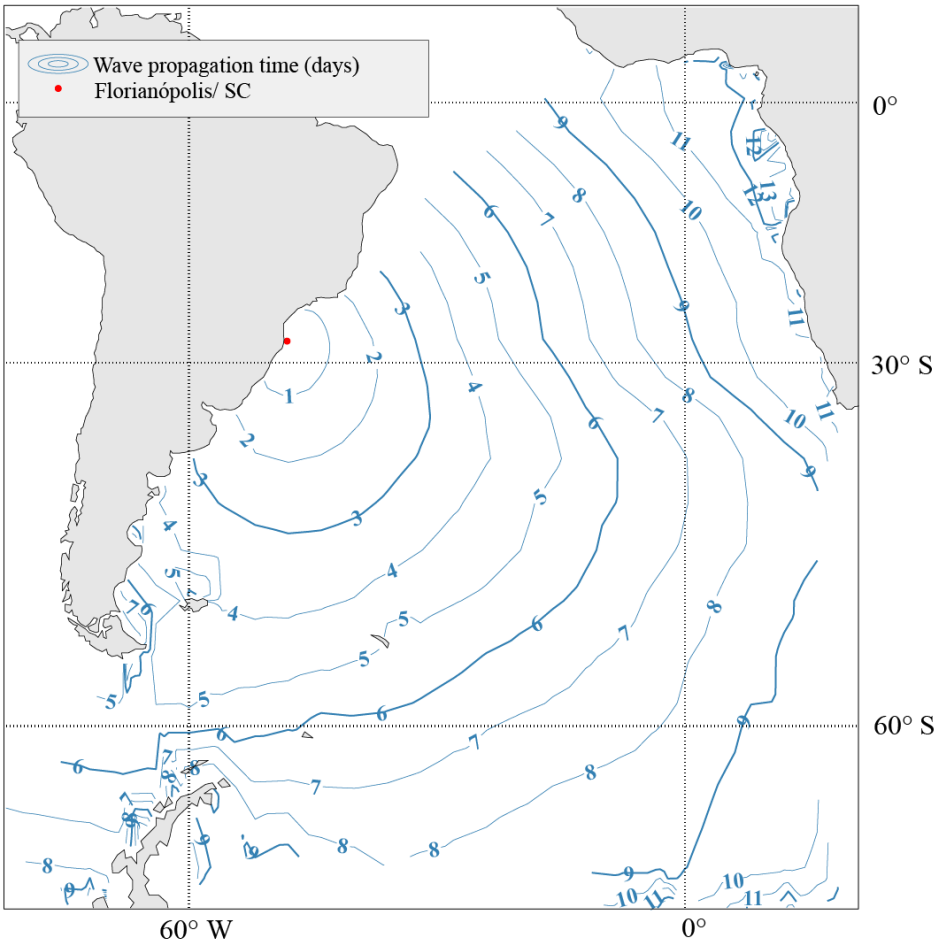

Figure 1: Isochrones of wave (blue lines) obtained from ESTELA. The red dot marks the position of the City of Florianópolis/SC, Brazil (Gomes da Silva et al., 2023)

Based on the wave propagation time, the maps of daily SLP and SLPG fields were modified in a way that in the areas where waves take an average of 2 days to reach the coast, SLP and SLPG data of t-2 days were used; for zones where generated waves take 3 days to reach the coast, SLP and SLPG from t-3 days was used, and so on.

The modified SLP and SLPG fields were organized in a single matrix [SLP SLPG] and the singular value decomposition (SVD) of the matrix was computed, in order to reduce the dimensionality of the dataset. Only the principal components (PCs) that represented 99% of the variability of the dataset were used. The dimension was reduced from a total of 2186 to 597 PCs.

The k-means algorithm was applied to the matrix of PCs in order to group similar atmospheric conditions into classes. Each class was then, characterized by a prototype that represents the centroid of the cluster, the so-called weather type (WT). This method requires the user to define the number of clusters (N) in which the dataset will be grouped in. Here, the optimal number of clusters was defined based on a sensitivity analysis (not shown) in which different N were tested and N=25 showed the best result when considering the following criterions: i) the number of

datasets should be higher than 50 in all clusters to allow statistical relationships to be stablished in subsequent analyses; ii) we looked for the higher Euclidean Distance between clusters; and iii) for the lower Euclidean Distance within the dataset of each cluster.

Figure 2 shows the 25 WTs identified (represented in SLP anomalies) and the respective probability of occurrence (right panel). The later was calculated using the number of data associated with each weather type. The objective of the figure is to highlight patterns of high and low pressure, hence the anomaly variable of pressure is utilized.

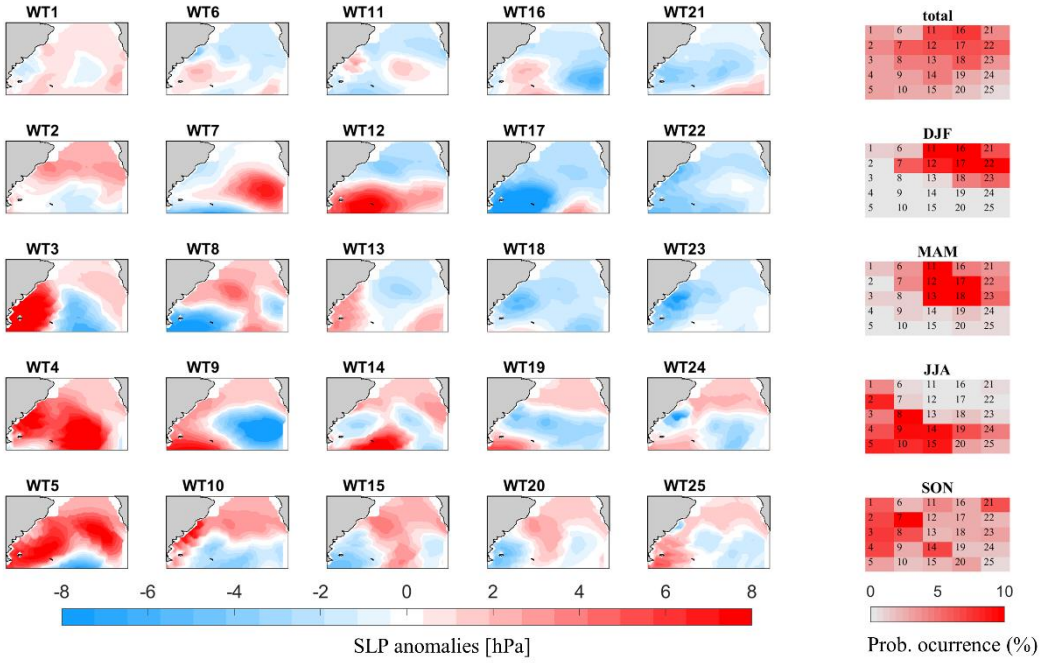

Figure 2: Weather types based on sea level pressure fields. The figure depicts pressure anomalies present in 99% of the data, as analyzed by Principal Component Analysis. The anomaly variable was chosen to highlight patterns of high and low pressure. Adjacent panels show the probabilities of occurrence for each weather type across all seasons and separately for DJF (winter), MAM (spring), JJA (summer), and SON (autumn).

2.3.2. Evaluation of the performance of GCMs

The SLP and SLPG data from GCMs were organized in a matrix with the same structure than the one used to define the weather types [SLP SLPG]. Next, the daily fields were projected on the weather types and the data from each day were associated with the weather type that was the most similar to it. The similarity between daily atmospheric patterns and the weather types was calculated using the Euclidean norm.

The number of data associated with each weather type was used to estimate the probability of occurrence from the projections for the historical period (1979-2004) and three future horizons: short-term (2015-2039), mid-term (2040-2069), and long-term (2070-2100). The following

analyses were carried out using the probability of occurrence obtained from the reanalysis, from the historical period and from the future horizons.

2.3.2.1. Historical

The similarity between the probabilities obtained from CFSR and from GCM's were evaluated using the scatter index of the mean squared error normalized by the mean probability (SI) (Equation 1) and the relative entropy (RE) (Equation 2).

$$SI = \sqrt{\frac{\sum_{i=1}^{N}(p_i - p_i')^2}{N}} \Bigg/ \left(\frac{\sum_{i=1}^{N} p_i}{N}\right), \quad (1)$$

$$RE = \sum_{i=1}^{N} p_i \left| log \frac{p_i}{p_i'} \right|, \quad (2)$$

where pi is the relative probability of the ith weather type from the reanalysis data; pi' is the relative probability of the ith weather type from a GCM simulation, and N is the number of weather types.

2.3.2.2. Seasonal

To assess the skill of the GCMs to reproduce interannual variability, the annual standard deviation of the probabilities obtained from the reanalysis data and those from the GCMs simulations were compared. The performance of the models was measured through the standard deviation scatter index (stdSI) (Equation 3) (Figure 3 column 1c).

$$stdSI = \sqrt{\frac{\sum_{i=1}^{N}(std(p_i) - std(p_i'))^2}{N}} \Bigg/ \frac{\sum_{i=1}^{N}(std(p_i))}{N}, \quad (3)$$

where $std()$ represents the standard deviation of the argument.

2.3.2.3. Future

The data from future projections was evaluated in terms of consistency when compared to the results obtained from other models. In this analysis, the magnitude of the changes in the probabilities of each weather type were used. The magnitude of the changes was obtained through the SI (Equation 1). For each model and scenario, the SI between the probability of future projections and the probability of the historical period from the same model were estimated. Inconsistent projections were considered those with SI outside the range of three standard deviations of the SI from the set of models.

For the results from those projections that were considered consistent, the magnitude of changes in the probability of occurrence over the historical period were also calculated. The relative percentage of change was estimated for each scenario in relation to the results for the same scenarios in the historical period.

3. Results and Discussion

3.1. Performance of GCMs

Figure 3 shows the 48 selected models and their respective performances. The columns "1. Historical" and "2. Seasonal" shows the comparison with CFSR reanalysis data between 1979 to 2004. Lower RE (Figure 3, 1.a) and SI (Figure 3, 1.b) indicate better performance when describing historical and seasonal probabilities, while lower stdSI (Figure 3, 1.c) indicate better performance on describing interannual variability.

The future projections section in Figure 3 shows the SI of each model for each scenario (in colors) and time interval (columns). The dark gray band between black lines within each column indicates the range of the three standard deviations filter that was applied to identify outliers, projections outside this range are considered inconsistent. Next, the results will be discussed by category of analysis.

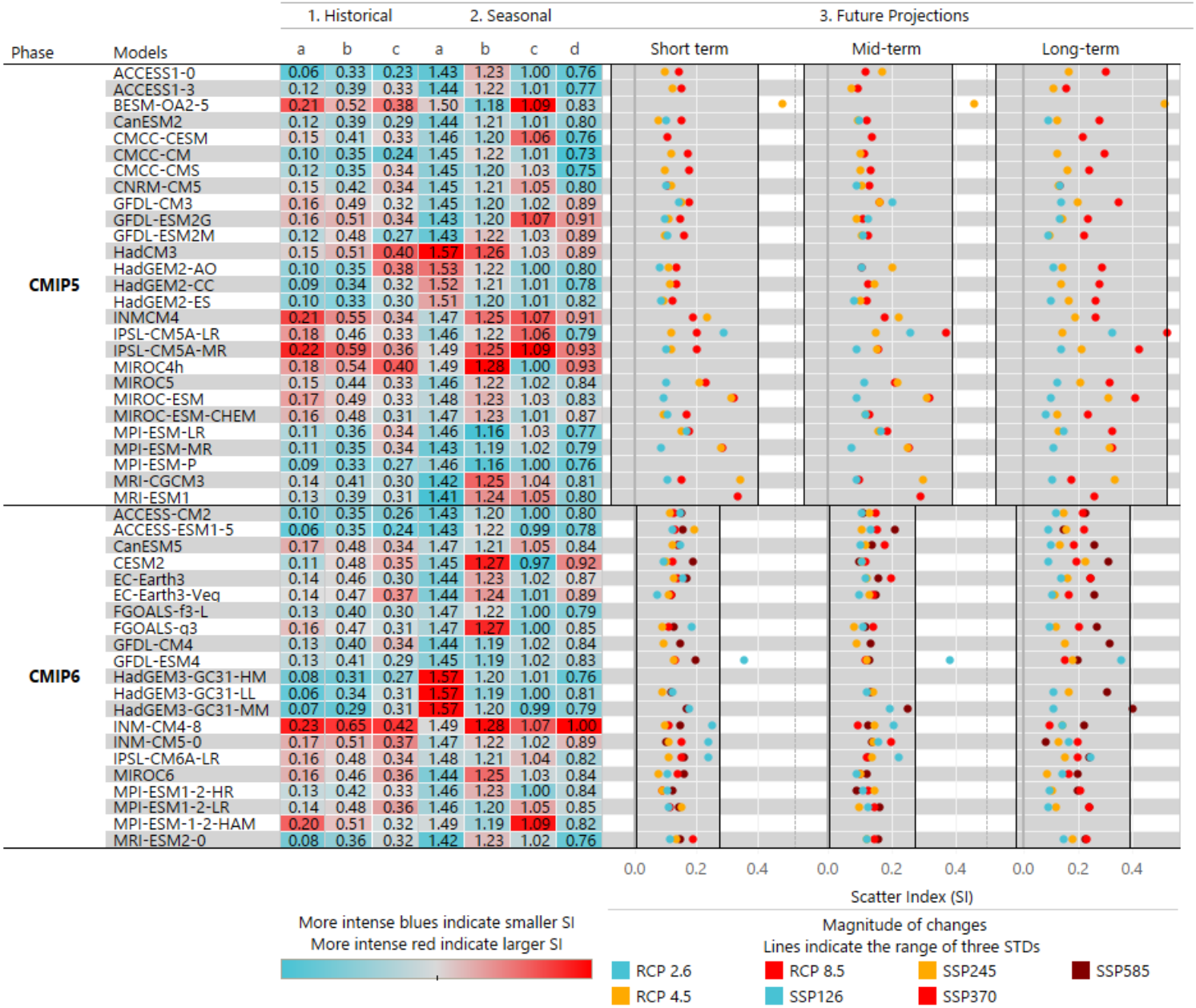
1. Historical
2. Seasonal
3. Future Projections
Phase
Models
a b c a b c d
Short term
Mid-term
Long-term
CMIP5
ACCESS1-0 0.06 0.33 0.23 1.43 1.23 1.00 0.76
ACCESS1-3 0.12 0.39 0.33 1.44 1.22 1.01 0.77
BESM-OA2-5 0.21 0.52 0.38 1.50 1.18 1.09 0.83
CanESM2 0.12 0.39 0.29 1.44 1.21 1.01 0.80
CMCC-CESM 0.15 0.41 0.33 1.46 1.20 1.06 0.76
CMCC-CM 0.10 0.35 0.24 1.45 1.22 1.01 0.73
CMCC-CMS 0.12 0.35 0.34 1.45 1.20 1.03 0.75
CNRM-CM5 0.15 0.42 0.34 1.45 1.21 1.05 0.80
GFDL-CM3 0.16 0.49 0.32 1.45 1.20 1.02 0.89
GFDL-ESM2G 0.16 0.51 0.34 1.43 1.20 1.07 0.91
GFDL-ESM2M 0.12 0.48 0.27 1.43 1.22 1.03 0.89
HadCM3 0.15 0.51 0.40 1.57 1.26 1.03 0.89
HadGEM2-AO 0.10 0.35 0.38 1.53 1.22 1.00 0.80
HadGEM2-CC 0.09 0.34 0.32 1.52 1.21 1.01 0.78
HadGEM2-ES 0.10 0.33 0.30 1.51 1.20 1.01 0.82
INMCM4 0.21 0.55 0.34 1.47 1.25 1.07 0.91
IPSL-CM5A-LR 0.18 0.46 0.33 1.46 1.22 1.06 0.79
IPSL-CM5A-MR 0.22 0.59 0.36 1.49 1.25 1.09 0.93
MIROC4h 0.18 0.54 0.40 1.49 1.28 1.00 0.93
MIROC5 0.15 0.44 0.33 1.46 1.22 1.02 0.84
MIROC-ESM 0.17 0.49 0.33 1.48 1.23 1.03 0.83
MIROC-ESM-CHEM 0.16 0.48 0.31 1.47 1.23 1.01 0.87
MPI-ESM-LR 0.11 0.36 0.34 1.46 1.16 1.03 0.77
MPI-ESM-MR 0.11 0.35 0.34 1.43 1.19 1.02 0.79
MPI-ESM-P 0.09 0.33 0.27 1.46 1.16 1.00 0.76
MRI-CGCM3 0.14 0.41 0.30 1.42 1.25 1.04 0.81
MRI-ESM1 0.13 0.39 0.31 1.41 1.24 1.05 0.80
CMIP6
ACCESS-CM2 0.10 0.35 0.26 1.43 1.20 1.00 0.80
ACCESS-ESM1-5 0.06 0.35 0.24 1.43 1.22 0.99 0.78
CanESM5 0.17 0.48 0.34 1.47 1.21 1.05 0.84
CESM2 0.11 0.48 0.35 1.45 1.27 0.97 0.92
EC-Earth3 0.14 0.46 0.30 1.44 1.23 1.02 0.87
EC-Earth3-Veg 0.14 0.47 0.37 1.44 1.24 1.01 0.89
FGOALS-f3-L 0.13 0.40 0.30 1.47 1.22 1.00 0.79
FGOALS-g3 0.16 0.47 0.31 1.47 1.27 1.00 0.85
GFDL-CM4 0.13 0.40 0.34 1.44 1.19 1.02 0.84
GFDL-ESM4 0.13 0.41 0.29 1.45 1.19 1.02 0.83
HadGEM3-GC31-HM 0.08 0.31 0.27 1.57 1.20 1.01 0.76
HadGEM3-GC31-LL 0.06 0.34 0.31 1.57 1.19 1.00 0.81
HadGEM3-GC31-MM 0.07 0.29 0.31 1.57 1.20 0.99 0.79
INM-CM4-8 0.23 0.65 0.42 1.49 1.28 1.07 1.00
INM-CM5-0 0.17 0.51 0.37 1.47 1.22 1.02 0.89
IPSL-CM6A-LR 0.16 0.48 0.34 1.48 1.21 1.04 0.82
MIROC6 0.16 0.46 0.36 1.44 1.25 1.03 0.84
MPI-ESM1-2-HR 0.13 0.42 0.33 1.46 1.23 1.00 0.84
MPI-ESM1-2-LR 0.14 0.48 0.36 1.46 1.20 1.05 0.85
MPI-ESM-1-2-HAM 0.20 0.51 0.32 1.49 1.19 1.09 0.82
MRI-ESM2-0 0.08 0.36 0.32 1.42 1.23 1.02 0.76
0.0 0.2 0.4 0.0 0.2 0.4 0.0 0.2 0.4
Scatter Index (SI)
More intense blues indicate smaller SI
More intense red indicate larger SI
Magnitude of changes
Lines indicate the range of three STDs
RCP 2.6
RCP 4.5
RCP 8.5
SSP126
SSP245
SSP370
SSP585

Figure 3 – Summary of the performance of the 48 global climate models. The column "1. Historical" presents (a) relative entropy (RE), (b) scatter index (SI), and (c) standard deviation of the scatter index (stdSI) between the CFSR reference probabilities and those simulated by the models. The column "2. Seasonal" presents the scatter index (SI) values for each model in each season, where (a) represents the summer months (DJF), (b) autumn (MAM), (c) winter (JJA), and (d) the spring months (SON). The intense blues indicate better performance of the model (lower SI), and the intense reds, worse performance (higher SI). The color scale is comparative between models (vertically), for each column the numerical scale is different. The column "3. Future Projections" shows the scatter index (SI) (colored dots on the graph) between the probabilities simulated and projected by each model for each period (short, mid, and long-term) and scenario (see color legend). The gray bars bounded by the black lines indicate the limit of three standard deviations for each CMIP phase. Please note that not all GCMs presented projections for all scenarios (see Table 1).

3.1.1. Historical analysis

The mean values of the analyzed indices showed no differences in performance between the CMIP5 (SI = 0.43, RE = 0.14) and CMIP6 (SI = 0.43, RE = 0.13) models, as verified in other works using CMIP3 and CMIP5 (Perez et al., 2014, Li et al., 2020, Ortega et al., 2021).

The HadGEM2-ES (SI = 0.33, RE = 0.10), ACCESS1-0 (SI = 0.33, RE = 0.06), MPI-ESM-P (SI = 0.33, RE = 0.09), HadGEM2-CC (SI = 0.34, RE = 0.09), and CMCC-C (SI = 0.35, RE = 0.10) models exhibited the lowest SI values among the CMIP5 models. In contrast, the HadCM3, GFDL-ESM2G, BESM-AO2-5, MIROC4h, INMCM4, and IPSL-CM5A-MR models showed the highest values.

The HadGEM3-GC31-MM (SI = 0.29, RE = 0.07), HadGEM3-GC31-HM (RI = 0.31, RE = 0.08), HadGEM3-GC31-LL (SI = 0, 34, RE = 0.06), ACCESS-ESM1-5 (SI = 0.35, RE = 0.06) and ACCESS-CM2 (SI = 0.35, RE = 0.10) presented the closest simulations when compared to reanalysis. While the MPI-ESM-1-2-HAM models and the INM-CM model versions 5-0 and 4-8 presented SI greater than 0.5, indicating that the modeled values are further from the reanalysis data. The other models presented SI between 0.39 and 0.48.

The results are consistent with those verified by Perez et al. (2014) for the Northern Hemisphere. For the CMIP5 model runs: ACCESS1.0, HadGEM2-CC, HadGEM2-ES, MPI-ESM-P and CMCC-CM were the models that presented the best performance for the South Atlantic, as well as the North Atlantic, according to Perez et al. (2014). On average, the CMIP5 models showed lower SI and RE in this analysis for the South Atlantic, compared to the North Atlantic results. In the mean values, the CMIP5 models showed lower SI and RE in this analysis for the South Atlantic (SI = 0.43, RE = 0.14), compared to the North Atlantic results (SI = 0.61, RE = 0.34) (Perez et al., 2014).

3.1.2. Seasonal analysis

Regarding the seasonal aspect, there is less significant differences between the models. The significant reduction in the amount of data analyzed should be considered, since the analysis is based on the probability of occurrence of weather types. This reduction could explain the smoothing of the differences between the performance of the models in the seasonal analysis.

During summer, the MRI-ESM1 (SI = 1.411) and MRI-CGCM3 (SI = 1.422) models of the CMIP5 and MRI-ESM2-0 (SI = 1.424) and ACCESS-ESM1-5 (SI = 1.429) of the CMIP6 presented the best performances. While, the CMIP5 results from HadGEM2-AO (SI = 1.53) and HadCM3 (SI = 1.568) and the CMIP6 results from HadGEM3-GC31-HM (SI = 1.566) and HadGEM3-GC31-LL (SI = 1.567) had the poorest performances. The SI average was the highest for the summer among all of the seasons for CMIP5 and CMIP6 (SI = 1.464 and 1.471, respectively).

The best performance was for the MIROC4h and MPI-ESM-P models (SI = 0.995 and 0.999, respectively) for the CMIP5 and for the CMIP6 of the CESM2 and HadGEM3-GC31-MM models (SI = 0.972 and 0.988, respectively), during autumn. The worst performances during this season were obtained the CMIP5 models IPSL-CM5A-MR and BESM-AO2-5 (SI = 1.089 for both) and the CMIP6 models INM-CM4-8 (SI = 1.067) and MPI-ESM-1-2- HAM (SI = 1.085).

The performance of both the CMIP5 and CMIP6 models for the summer and autumn months was reduced compared to the performance during the winter and spring months. As shown in other works (Adam et al., 2016, Adam et al., 2018, Tian & Dong, 2020, Ortega et al., 2021) this behavior may occur due to the double-ITCZ bias (Intertropical Convergence Zone), which is not limited only to this region, but is recurrent in the representation of this period by ocean-atmosphere coupled models.

During the winter months, the CMIP5 models: MPI-ESM-LR, MPI-ESM-P and BESM-OA2-5 presented the lowest SI (1.155, 1.163 and 1.177, respectively). The highest SI were associated with HadCM3 and MIROC4h models (SI = 1.257 and 1.278). Among the CMIP6 models, the best performances were achieved by GFDL-ESM4 (SI = 1.187) and HadGEM3-GC31-LL (SI = 1.188) and the worst performances by CESM2 (SI = 1.271) and INM-CM4-8 (SI = 1.276).

The spring simulations showed the lowest SI average for both the CMIP5 and CMIP6 models (SI = 0.823 and 0838, respectively). The best results from the CMIP5 models were obtained from the two versions of CMCC (CM and CMS), with SI equal to 0.732 (CM) and 0.748 (CMS). The worst performances were for the MIROC4h (SI = 0.926) and IPSL-CM5A-MR (SI = 0.928) models. For CMIP6, the best models were HadGEM3-GC31-HM (SI = 0.759) and MRI-ESM2-0 (SI = 0.763) and the worst were CESM2 (SI = 0.921) and INM-CM4-8 (SI = 1.001).

3.1.3. Interannual variability

The interannual variabilities of the model´s results were evaluated by computing the standard deviation of the annual probabilities of occurrence of each weather type (Eq. 3), once again the ACESS1-0 model (SI = 0.232) presented the best performance, followed by the CMCC-CM models (SI = 0.239), GFDL-ESM2M (SI = 0.268) and MPI-ESM-P (SI = 0.272), for CMIP5. The mean SI for the CMIP5 models was 0.325. For the CMIP6 models, the two versions of the ACCESS model (ESM1-5 and CM2) presented the best performances (SI = 0.236 and 0.261, respectively), followed by HadGEM3-GC31-HM (SI = 0.272) and GFDL-ESM4 (SI = 0.293). The mean SI for the CMIP6 models was 0.324, similar to the CMIP5 models.

It is observed that for both phases of CMIP, there were variations in the models with the best and worst performance considering the evaluation of the complete historical period and the evaluation of seasonal and interannual variability. Reinforcing that in some cases the performance of the models may vary according to the season, as already pointed out by Perez et al. (2014). Another study using a methodology for classifying atmospheric circulation patterns, similar to the one used in the present work, was directed by Fernadez-Granja et al. (2021) and also identified a similar behavior of the models when reproducing the circulation patterns. Although, in general, they identified an improvement in the CMIP6 models, there is great variability in the evaluation of the individual performance of each model.

Thus, the choice of the most suitable model for an analysis may vary according to the objectives of the analysis. However, the HadGEM and ACCESS models stand out in all their versions and also the performance of the MPI-ESM-P and CMCC-CM models among the CMIP5 models and the GFDL-ESM4 and MRI-ESM2-0 from the CMIP6 models.

3.1.4. Consistency analysis

The future projections of the selected models were evaluated based on their consistency. The SI (Eq. 1) was calculated between the probabilities of occurrence simulated by the models in the historical period and those projected in each scenario. In Figure 3, in column “3. Future Projections”, the SI for each model and scenario are presented. The range delimited by two black lines within each time interval (short, mid, long) indicates the interval of three standard deviations from the SI mean of the models for that period.

By measuring the distance between current (historical) frequencies and future (projected) frequencies, the SI quantifies the magnitude of changes estimated by future projections. This assessment highlights the limitation of the methodology in not projecting new patterns but only indicating changes in the frequency of weather types already identified in the historical period. Therefore, this study will not evaluate the weather types themselves but rather the ability of the models to simulate future projections based on the consistency of these projections across different phases of the CMIP, models, and scenarios.

For the CMIP5 runs, only the BESM-OA2-5 model presented SI greater than three standard deviations from the mean for the short and medium term in the RCP4.5 scenario. As for the CMIP6 simulations, the GFDL-ESM4 model presented SI out of range for the short and medium term in the SSP126 scenario. Also, the HadGEM3-GC31-MM model was outside the range of three standard deviations for the long term in the SSP585 scenario.

For the other models, it is observed that the CMIP6 projections are more consistent among the analyzed models, signaled by the smaller standard deviation between the projections for each period of time. Similar results are found in Harvey et al. (2020), who show that the magnitude of bias in CMIP6 models are significantly smaller compared to previous phases. In Curtis et al. (2020), the authors found evidence, based on the improved horizontal resolution of the models, that the CMIP6 models can provide more realistic projections of climate change in the Southern Hemisphere. For Tokarska et al. (2020), the CMIP6 results are consistent, even if different, with previous assessments based on CMIP5.

As expected, the projections of the RCP2.6 and SSP126 scenarios have a lower SI, in general, that is, they are closer to the current values, while the RCP8.5 and SSP585 scenarios, in general, presented higher SI. It is noteworthy that the comparative analysis of performance between the CMIP5 and CMIP6 models also depends on the variable used, as verified in the paper by Song et al. (2021). In this analysis, considering the reproduction of weather types based on sea level pressure, the CMIP6 models present a much narrower band of three standard deviation (the gray bands in Fig. 3) than the CMIP5 models. While this is good news for the climate modeling community, Wyser et al. (2020), note that the comparison of the results of CMIP5 and CMIP6 should be done with caution, given the difference between the models themselves and the forcing conditions.

3.2. Future projections

The difference between the probabilities of occurrence of each weather type for the historical period and the future projections of each scenario was estimated through the average of the results from all consistent models. Although not strictly comparable due to their fundamental characteristics, it is possible to analyze the scenarios of both CMIP5 and CMIP6 in general terms. It is worth noting that the main difference between the scenarios lies in the factors they address, with SSP scenarios considering not only greenhouse gas emissions but also broader socio-economic factors. Thus, the scenarios were categorized into low emission scenarios (RCP 2.6 and SSP126), intermediate emission scenarios (RCP 4.5, SSP245, and SSP370), and high emission scenarios (RCP 8.5 and SSP585); for short-term (2015-2039), mid-term (2040-2069), and long-term (2070-2100), as shown in Figure 4.

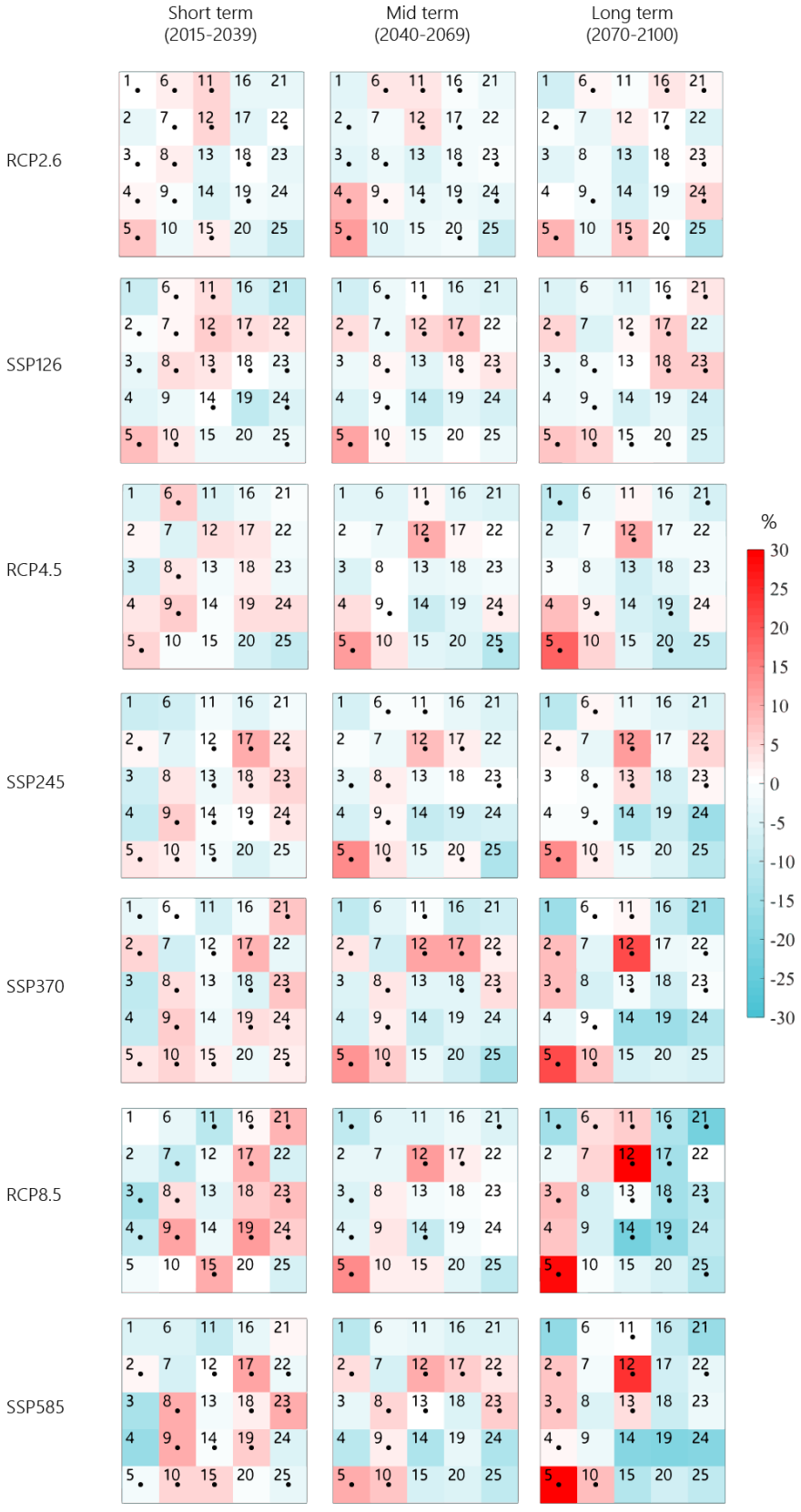

Figure 4: Average changes in the probability of each weather type (WT) projected for each scenario and time interval. Inconsistent projections were not considered in the analysis. The black dots indicate agreement in the sign of change (increase or decrease) between more than 80% of the models. The scale indicates the change relative to the historical period in percentage.

Considering the RCP2.6 and SSP126 scenarios, for the short and mid-term, both projections mainly indicated an increase in the probabilities of occurrence of WT12 and WT5. Considering the short term, there is also an indication of the reduction of the probabilities of occurrence of WT16 and WT21, weather types that are frequent for the historical period. For the long term, all changes are less intense for both scenarios. It is noticeable a regularity in the weather types that change in different scenarios and periods of time. As an example, WT5, WT12 and WT17 increase their probabilities of occurrence and the WT7 and WT16 present a reduction of their probabilities of occurrence.

For scenarios RCP4.5, SSP245 and SSP370, in the short term, the three scenarios agree on the increase of their probabilities of occurrence of WT9 and WT17, in addition to WT5 and WT12, which are similar to the results of scenarios RCP2.6 and SSP126. In these scenarios, there is also mainly a reduction of the probabilities of occurrence of WT3, WT7 and WT11. For the mid and long term, these scenarios point to an increase in the probability of occurrence of WT5 and WT12, especially the SSP370 scenario, in the long term, which indicates a more significant increase in the probability of WT12. A reduction in the probability of occurrence of WT7 and WT16 is also pointed out in these scenarios.

According to Harvey et al. (2020), the response of the CMIP6 models to the SSP245 scenario is greater than that of the CMIP5 models to the RCP4.5 scenario. However, in the methodology used in the present work, no significant difference was identified in the intensity of the results of the RCP4.5 and SSP245 scenarios.

In the RCP8.5 and SSP585 scenarios, more intense changes are verified than those observed in the other scenarios. For the short term, both scenarios show an increase of their probabilities of occurrence of WT9, WT17 and WT19. There is agreement regarding the reduction in the probability of WT3, WT4 and WT11. For the mid-term, the behavior is similar in both scenarios. The main probabilities increase is associated with WT12 and then with WT5. The reductions are less intense, but again associated with the WT1, WT7 and WT16. In the long term, the pattern of variations is similar, but the changes are more intense. For both scenarios there is a significant increase in the probability of occurrence of WT12 and also, to a lesser extent, of WT5. The probability reduction is greater in the WT16 for both scenarios.

4. Summary and conclusion

The Bureau of Meteorology and Commonwealth Scientific and Industrial Research Organization (ACCESS), and Hadley Centre for Climate Prediction and Research (HadGEM) models showed the best performances in general in reproducing the historical synoptic conditions. Except for the

models ACCESS1-3 and HadCM3, from CMIP5, the other models of the mentioned centers, both for CMIP5 and for CMIP6, presented a maximum SI of 0.35 and a maximum RE of 0.10.

In average, the results from CMIP5 and CMIP6 showed similar performances. However, some improvements for CMIP6 can be noted when assessing the results from each model individually. For instance, the model GFDL-CM4 (SI = 0.40 and RE = 0.13) showed improvement in relation to GFDL-CM3 (SI = 0.49 and RE = 0.16), the INM-CM5-0 (SI = 0.51 and RE = 0.17) showed improvement in relation to INM- CM4 (SI = 0.55 and RE = 0.21), and MRI-ESM2-0 (SI = 0.36 and RE = 0.08) showed improvement in relation to MRI-ESM1 (SI = 0.39 and RE = 0.13).

Regarding the seasonality, it was observed that the performance of the models depends on the season and is not necessarily related to the performance in the historical period, as also noted by Perez et al. (2014). For example, our results show that the HadGEM models, which performed well in the historical analysis (SI less than 0.5 and RE less than or equal to 0.10), performed poorly when estimating the seasonal probability, especially during the summer (SI greater than 1.50). From this, it can be concluded that the choice of the most appropriate models may vary according to the purpose of the analysis.

The consistency of future projections was evaluated from the limit of three standard deviations from the average SI of the magnitude of changes in all projections. In this analysis, the BESM-AO2-5 model showed an inconsistent magnitude of change in relation to the other CMIP5 models for the short and mid-term in the RCP4.5 scenario. In the SSP 1 scenario, the GFDL-ESM4 model also showed inconsistency for the short and mid-term, while the HadGEM3-GC31-MM model presented for the long term in the SSP585 scenario. The good news is the improvement on consistency of the CMIP6 models compared to the CMIP5 models. As in other works (Garzoli & Matano, 2011), our results reinforce the need for further studies in the South Atlantic regarding future projections using climate models.

The application of this methodology of analysis of climate models based on weather types proved to be consistent with the results obtained by other studies in the region. This approach also makes it possible, for further studies, to evaluate meteoceanographic variables and their future projections through statistical downscaling methods.

Acknowledgments

The authors would like to thank the climate modeling groups (listed in Figure 3 and Table 1 of this work) for making the results from different models available to the scientific community. Thanks also to the Federal University of Santa Catarina (UFSC) and the Graduate Program in Oceanography (PPGOceano) for their support in English text of this paper. Finally, the authors

thank the whole team of the Regional Oceanic and Atmospheric Downscaling Project (ROAD) and partner universities (Federal University of Rio Grande - FURG, Federal University of Rio Grande do Sul - UFRGS, and the University of Cantabria) for their contributions to the project discussions. This study was financed in part by the Coordenação de Aperfeiçoamento de Pessoal de Nível Superior - Brasil (CAPES) – Finance code 001 through grant 88887.145393 / 2017-00.

Conflict of interest

The authors declare that there is no competition of interests.

ORCID

L.B. 0000-0002-6776-3147

P.G. da S. 0000-0003-4766-8449

A.F. H. F. 0000-0003-4843-8557

F.J. M. 0000-0002-5005-1100

A.H.F.K. ahfklein@gmail.com

References

Abadi, A.M., Oglesby, R., Rowe, C., Mawalagedara, R., 2018. Evaluation of GCMs historical simulations of monthly and seasonal climatology over Bolivia. Clim Dyn 51, 733–754. https://doi.org/10.1007/s00382-017-3952-y

Adam, O., Schneider, T., Brient, F., Bischoff, T., 2016. Relation of the double-ITCZ bias to the atmospheric energy budget in climate models. Geophysical Research Letters, 43, 7670-7677. https://doi.org/10.1002/2016gl069465

Adam, O., Schneider, T., Brient, F., 2018. Regional and seasonal variations of the double-ITCZ bias in CMIP5 models. Clim Dyn 51, 101–117. https://doi.org/10.1007/s00382-017-3909-1

Alves, J. H. G. M., Melo, E., 2001. Measurement and modeling of wind waves at the northern coast of Santa Catarina, Brazil. Brazilian Journal of Oceanography, 49(1–2). https://doi.org/10.1590/s1679-87592001000100002

Andrews, T., Andrews, M.B., Bodas-Salcedo, A., Jones, G.S., Kuhlbrodt, T., Manners, J., Menary, M.B., Ridley, J., Ringer, M.A., Sellar, A.A., Senior, C.A., Tang, Y., 2019. Forcings, Feedbacks, and Climate Sensitivity in HadGEM3-GC3.1 and UKESM1. Journal of Advances in Modeling Earth Systems 11, 4377–4394. https://doi.org/10.1029/2019MS001866

Araújo, C. E. S., Franco, D., Melo, E., Pimenta, F. Wave regime characteristics of the southern Brazilian Coast. Proceedings of the Sixth International Conference on Coastal and Port Engineering in Developing Countries, COPEDEC VI, Colombo, Sri Lanka, Paper No. 097; pp 15, 2003.

Arora, V.K., Scinocca, J.F., Boer, G.J., Christian, J.R., Denman, K.L., Flato, G.M., Kharin, V.V., Lee, W.G., Merryfield, W.J., 2011. Carbon emission limits required to satisfy future representative concentration pathways of greenhouse gases. Geophysical Research Letters 38. https://doi.org/10.1029/2010GL046270

Berg, A., McColl, K.A., 2021. No projected global drylands expansion under greenhouse warming. Nat. Clim. Chang. 11, 331–337. https://doi.org/10.1038/s41558-021-01007-8

Bi, D., Dix, M., Marsland, S., O'Farrell, S., Rashid, H., Uotila, P., Hirst, A., Kowalczyk, E., Golebiewski, M., Sullivan, A., Yan, H., Hannah, N., Franklin, C., Sun, Z., Vohralik, P., Watterson, I., Zhou, X., Fiedler, R., Collier, M., Ma, Y., Noonan, J., Stevens, L., Uhe, P., Zhu, H., Griffies, S., Hill, R., Harris, C., Puri, K., 2013. The ACCESS coupled model: description, control climate and evaluation. Australian Meteorological and Oceanographic Journal 63, 41–64. https://doi.org/10.22499/2.6301.004

Bi, D., Dix, M., Marsland, S., O'Farrell, S., Sullivan, A., Bodman, R., Law, R., Harman, I., Srbinovsky, J., Rashid, H.A., Dobrohotoff, P., Mackallah, C., Yan, H., Hirst, A., Savita, A., Dias, F.B., Woodhouse, M., Fiedler, R., Heerdegen, A., 2020. Configuration and spin-up of ACCESS-CM2, the new generation Australian Community Climate and Earth System Simulator Coupled Model. Journal of Southern Hemisphere Earth Systems Science 70, 225–251.

Bidegain, M., 2006. Performance of GCMs and climate future scenarios for southeastern South America, in: Proceedings of 8 ICSHMO. Presented at the International Conference on Southern Hemisphere Meteorology and Oceanography, INPE, Foz do Iguaçu, Brazil, pp. 223–226.

Bock, L., Lauer, A., Schlund, M., Barreiro, M., Bellouin, N., Jones, C., Meehl, G.A., Predoi, V., Roberts, M.J., Eyring, V., 2020. Quantifying Progress Across Different CMIP

536 Phases With the ESMValTool. Journal of Geophysical Research: Atmospheres 125,
537 e2019JD032321. https://doi.org/10.1029/2019JD032321
538 Boucher, O., Servonnat, J., Albright, A.L., Aumont, O., Balkanski, Y., Bastrikov, V., Bekki,
539 S., Bonnet, R., Bony, S., Bopp, L., Braconnot, P., Brockmann, P., Cadule, P., Caubel,
540 A., Cheruy, F., Codron, F., Cozic, A., Cugnet, D., D'Andrea, F., Davini, P., Lavergne,
541 C. de, Denvil, S., Deshayes, J., Devilliers, M., Ducharne, A., Dufresne, J.-L., Dupont,
542 E., Éthé, C., Fairhead, L., Falletti, L., Flavoni, S., Foujols, M.-A., Gardoll, S.,
543 Gastineau, G., Ghattas, J., Grandpeix, J.-Y., Guenet, B., Guez, L., E., Guilyardi, E.,
544 Guimberteau, M., Hauglustaine, D., Hourdin, F., Idelkadi, A., Joussaume, S.,
545 Kageyama, M., Khodri, M., Krinner, G., Lebas, N., Levavasseur, G., Lévy, C., Li, L.,
546 Lott, F., Lurton, T., Luyssaert, S., Madec, G., Madeleine, J.-B., Maignan, F., Marchand,
547 M., Marti, O., Mellul, L., Meurdesoif, Y., Mignot, J., Musat, I., Ottlé, C., Peylin, P.,
548 Planton, Y., Polcher, J., Rio, C., Rochetin, N., Rousset, C., Sepulchre, P., Sima, A.,
549 Swingedouw, D., Thiéblemont, R., Traore, A.K., Vancoppenolle, M., Vial, J., Vialard,
550 J., Viovy, N., Vuichard, N., 2020. Presentation and Evaluation of the IPSL-CM6A-LR
551 Climate Model. Journal of Advances in Modeling Earth Systems 12, e2019MS002010.
552 https://doi.org/10.1029/2019MS002010
553 Cagigal, L., Rueda, A., Castanedo, S., Cid, A., Perez, J., Stephens, S.A., Coco, G., Méndez,
554 F.J., 2020. Historical and future storm surge around New Zealand: From the 19th
555 century to the end of the 21st century. International Journal of Climatology 40, 1512–
556 1525. https://doi.org/10.1002/joc.6283
557 Campos, R.M., Camargo, R.D., Harari, J., 2010. Caracterização de eventos extremos do
558 nível do mar em Santos e sua correspondência com as reanálises do modelo do NCEP
559 no sudoeste do Atlântico Sul. Rev. bras. meteorol. 25, 175–184.
560 https://doi.org/10.1590/S0102-77862010000200003
561 Camus, P., Losada, I.J., Izaguirre, C., Espejo, A., Menéndez, M., Pérez, J., 2017. Statistical
562 wave climate projections for coastal impact assessments: statistical wave climate
563 projections. Earth's Future 5, 918–933. https://doi.org/10.1002/2017EF000609
564 Camus, P., Menéndez, M., Méndez, F.J., Izaguirre, C., Espejo, A., Cánovas, V., Pérez, J.,
565 Rueda, A., Losada, I.J., Medina, R., 2014. A weather-type statistical downscaling
566 framework for ocean wave climate. J. Geophys. Res. Oceans 119, 7389–7405.
567 https://doi.org/10.1002/2014JC010141

Carrère, L., Lyard, F., 2003. Modeling the barotropic response of the global ocean to atmospheric wind and pressure forcing - comparisons with observations. Geophysical Research Letters 30. https://doi.org/10.1029/2002GL016473

Cherchi, A., Ambrizzi, T., Behera, S., Freitas, A.C.V., Morioka, Y., Zhou, T., 2018. The Response of Subtropical Highs to Climate Change. Curr Clim Change Rep 4, 371–382. https://doi.org/10.1007/s40641-018-0114-1

Collins, W.J., Bellouin, N., Doutriaux-Boucher, M., Gedney, N., Hinton, T., Jones, C.D., Liddicoat, S., Martin, G., O'Connor, F., Rae, J., Senior, C., Totterdell, I., Woodward, S., Reichler, T., Kim, J., 2008. Evaluation of HadGEM2 model. Met Office Hadley Centre, Technical Note No. HCTN 74. http://www.metoffice.gov.uk/publications/HCTN/index.html

Curtis, P.E., Ceppi, P., Zappa, G., 2020. Role of the mean state for the Southern Hemispheric jet stream response to CO2 forcing in CMIP6 models. Environ. Res. Lett. 15. https://doi.org/10.1088/1748-9326/ab8331

Danabasoglu, G., Lamarque, J.-F., Bacmeister, J., Bailey, D.A., DuVivier, A.K., Edwards, J., Emmons, L.K., Fasullo, J., Garcia, R., Gettelman, A., Hannay, C., Holland, M.M., Large, W.G., Lauritzen, P.H., Lawrence, D.M., Lenaerts, J.T.M., Lindsay, K., Lipscomb, W.H., Mills, M.J., Neale, R., Oleson, K.W., Otto-Bliesner, B., Phillips, A.S., Sacks, W., Tilmes, S., Kampenhout, L. van, Vertenstein, M., Bertini, A., Dennis, J., Deser, C., Fischer, C., Fox-Kemper, B., Kay, J.E., Kinnison, D., Kushner, P.J., Larson, V.E., Long, M.C., Mickelson, S., Moore, J.K., Nienhouse, E., Polvani, L., Rasch, P.J., Strand, W.G., 2020. The Community Earth System Model Version 2 (CESM2). Journal of Advances in Modeling Earth Systems 12, e2019MS001916. https://doi.org/10.1029/2019MS001916

Davini, P., Cagnazzo, C., Fogli, P.G., Manzini, E., Gualdi, S., Navarra, A., 2014. European blocking and Atlantic jet stream variability in the NCEP/NCAR reanalysis and the CMCC-CMS climate model. Clim Dyn 43, 71–85. https://doi.org/10.1007/s00382-013-1873-y

Gomes da Silva, P., Dalinghaus, C., González, M., Gutiérrez, O., Espejo, A., Abascal, A.J., Klein, A.H.F., 2016. Estimating Flooding Level Through the Brazilian Coast Using Reanalysis Data. Journal of Coastal Research 1092–1096. https://doi.org/10.2112/SI75-219.1

Gomes da Silva, P.G., Borato, L., Fetter Filho, A.F.H., Mendez, F.J., Klein, A.H.F., 2023. *An atmospheric predictor to estimate the total water level at coasts with a shallow*

602 *continental shelf. Part 1: Predictor definition and application to characterize the local*
603 *marine climate.* [Manuscript in preparation].
604 Degola, T.S.D., 2013. Impactos e variabilidade do Anticiclone Subtropical do Atlântico Sul
605 sobre o Brasil no clima presente e em cenários futuros. In *Dissertação de Mestrado*, São
606 Paulo 112.
607 Donner, L.J., Wyman, B.L., Hemler, R.S., Horowitz, L.W., Ming, Y., Zhao, M., Golaz, J.-C.,
608 Ginoux, P., Lin, S.-J., Schwarzkopf, M.D., Austin, J., Alaka, G., Cooke, W.F.,
609 Delworth, T.L., Freidenreich, S.M., Gordon, C.T., Griffies, S.M., Held, I.M., Hurlin,
610 W.J., Klein, S.A., Knutson, T.R., Langenhorst, A.R., Lee, H.-C., Lin, Y., Magi, B.I.,
611 Malyshev, S.L., Milly, P.C.D., Naik, V., Nath, M.J., Pincus, R., Ploshay, J.J.,
612 Ramaswamy, V., Seman, C.J., Shevliakova, E., Sirutis, J.J., Stern, W.F., Stouffer, R.J.,
613 Wilson, R.J., Winton, M., Wittenberg, A.T., Zeng, F., 2011. The Dynamical Core,
614 Physical Parameterizations, and Basic Simulation Characteristics of the Atmospheric
615 Component AM3 of the GFDL Global Coupled Model CM3. Journal of Climate 24,
616 3484–3519. https://doi.org/10.1175/2011JCLI3955.1
617 Dufresne, J.-L., Foujols, M.-A., Denvil, S., Caubel, A., Marti, O., Aumont, O., Balkanski,
618 Y., Bekki, S., Bellenger, H., Benshila, R., Bony, S., Bopp, L., Braconnot, P.,
619 Brockmann, P., Cadule, P., Cheruy, F., Codron, F., Cozic, A., Cugnet, D., de Noblet,
620 N., Duvel, J.-P., Ethé, C., Fairhead, L., Fichefet, T., Flavoni, S., Friedlingstein, P.,
621 Grandpeix, J.-Y., Guez, L., Guilyardi, E., Hauglustaine, D., Hourdin, F., Idelkadi, A.,
622 Ghattas, J., Joussaume, S., Kageyama, M., Krinner, G., Labetoulle, S., Lahellec, A.,
623 Lefebvre, M.-P., Lefevre, F., Levy, C., Li, Z.X., Lloyd, J., Lott, F., Madec, G., Mancip,
624 M., Marchand, M., Masson, S., Meurdesoif, Y., Mignot, J., Musat, I., Parouty, S.,
625 Polcher, J., Rio, C., Schulz, M., Swingedouw, D., Szopa, S., Talandier, C., Terray, P.,
626 Viovy, N., Vuichard, N., 2013. Climate change projections using the IPSL-CM5 Earth
627 System Model: from CMIP3 to CMIP5. Clim Dyn 40, 2123–2165.
628 https://doi.org/10.1007/s00382-012-1636-1
629 Dunne, J.P., Horowitz, L.W., Adcroft, A.J., Ginoux, P., Held, I.M., John, J.G., Krasting, J.P.,
630 Malyshev, S., Naik, V., Paulot, F., Shevliakova, E., Stock, C.A., Zadeh, N., Balaji, V.,
631 Blanton, C., Dunne, K.A., Dupuis, C., Durachta, J., Dussin, R., Gauthier, P.P.G.,
632 Griffies, S.M., Guo, H., Hallberg, R.W., Harrison, M., He, J., Hurlin, W., McHugh, C.,
633 Menzel, R., Milly, P.C.D., Nikonov, S., Paynter, D.J., Ploshay, J., Radhakrishnan, A.,
634 Rand, K., Reichl, B.G., Robinson, T., Schwarzkopf, D.M., Sentman, L.T., Underwood,
635 S., Vahlenkamp, H., Winton, M., Wittenberg, A.T., Wyman, B., Zeng, Y., Zhao, M.,

2020. The GFDL Earth System Model Version 4.1 (GFDL-ESM 4.1): Overall Coupled Model Description and Simulation Characteristics. Journal of Advances in Modeling Earth Systems 12, e2019MS002015. https://doi.org/10.1029/2019MS002015

Dunne, J.P., John, J.G., Adcroft, A.J., Griffies, S.M., Hallberg, R.W., Shevliakova, E., Stouffer, R.J., Cooke, W., Dunne, K.A., Harrison, M.J., Krasting, J.P., Malyshev, S.L., Milly, P.C.D., Phillipps, P.J., Sentman, L.T., Samuels, B.L., Spelman, M.J., Winton, M., Wittenberg, A.T., Zadeh, N., 2012. GFDL's ESM2 Global Coupled Climate–Carbon Earth System Models. Part I: Physical Formulation and Baseline Simulation Characteristics. Journal of Climate 25, 6646–6665. https://doi.org/10.1175/JCLI-D-11-00560.1

Durrant, T., Greenslade, D., Hemer, M., Trenham, C., 2014. A Global Wave Hindcast focussed on the Central and South Pacific. In *CAWCR Technical Report* (Issue 70). http://www.cawcr.gov.au/technical-reports/CTR_070.pdf

Eyring, V., Bony, S., Meehl, G.A., Senior, C.A., Stevens, B., Stouffer, R.J., Taylor, K.E., 2016. Overview of the Coupled Model Intercomparison Project Phase 6 (CMIP6) experimental design and organization. Geoscientific Model Development 9, 1937–1958. https://doi.org/10.5194/gmd-9-1937-2016

Fant, C., Adam Schlosser, C., Strzepek, K., 2016. The impact of climate change on wind and solar resources in southern Africa. Applied Energy 161, 556–564. https://doi.org/10.1016/j.apenergy.2015.03.042

Fasullo, J.T., 2020. Evaluating simulated climate patterns from the CMIP archives using satellite and reanalysis datasets using the Climate Model Assessment Tool (CMATv1). Geoscientific Model Development 13, 3627–3642. https://doi.org/10.5194/gmd-13-3627-2020

Fasullo, J.T., Phillips, A.S., Deser, C., 2020. Evaluation of Leading Modes of Climate Variability in the CMIP Archives. Journal of Climate 33, 5527–5545. https://doi.org/10.1175/JCLI-D-19-1024.1

Fernandez-Granja, J.A., Casanueva, A., Bedia, J., Fernandez, J., 2021. Improved atmospheric circulation over Europe by the new generation of CMIP6 earth system models. Clim Dyn 56, 3527–3540. https://doi.org/10.1007/s00382-021-05652-9

Fogli, P.G., Manzini, E., Vichi, M., Alessandri, A., Patara, L., Gualdi, S., Scoccimarro, E., Masina, S., Navarra, A., 2009. INGV-CMCC Carbon (ICC): A Carbon Cycle Earth System Model (SSRN Scholarly Paper No. ID 1517282). Social Science Research Network, Rochester, NY. https://doi.org/10.2139/ssrn.1517282

Fowler, H.J., Blenkinsop, S., Tebaldi, C., 2007. Linking climate change modelling to impacts studies: recent advances in downscaling techniques for hydrological modelling. International Journal of Climatology 27, 1547–1578. https://doi.org/10.1002/joc.1556

Garzoli, S.L., Matano, R., 2011. The South Atlantic and the Atlantic Meridional Overturning Circulation. Deep Sea Research Part II: Topical Studies in Oceanography, Climate and the Atlantic Meridional Overturning Circulation 58, 1837–1847. https://doi.org/10.1016/j.dsr2.2010.10.063

Giorgetta, M.A., Jungclaus, J., Reick, C.H., Legutke, S., Bader, J., Böttinger, M., Brovkin, V., Crueger, T., Esch, M., Fieg, K., Glushak, K., Gayler, V., Haak, H., Hollweg, H.-D., Ilyina, T., Kinne, S., Kornblueh, L., Matei, D., Mauritsen, T., Mikolajewicz, U., Mueller, W., Notz, D., Pithan, F., Raddatz, T., Rast, S., Redler, R., Roeckner, E., Schmidt, H., Schnur, R., Segschneider, J., Six, K.D., Stockhause, M., Timmreck, C., Wegner, J., Widmann, H., Wieners, K.-H., Claussen, M., Marotzke, J., Stevens, B., 2013. Climate and carbon cycle changes from 1850 to 2100 in MPI-ESM simulations for the Coupled Model Intercomparison Project phase 5. Journal of Advances in Modeling Earth Systems 5, 572–597. https://doi.org/10.1002/jame.20038

Gordon, C., Cooper, C., Senior, C.A., Banks, H., Gregory, J.M., Johns, T.C., Mitchell, J.F.B., Wood, R.A., 2000. The simulation of SST, sea ice extents and ocean heat transports in a version of the Hadley Centre coupled model without flux adjustments. Climate Dynamics 16, 147–168. https://doi.org/10.1007/s003820050010

Gramcianinov, C. B., Campos, R. M., Guedes Soares, C., Camargo, R. de., 2020. Extreme waves generated by cyclonic winds in the western portion of the South Atlantic Ocean. Ocean Engineering, 213(January), 107745. https://doi.org/10.1016/j.oceaneng.2020.107745

Hall, A., Cox, P., Huntingford, C., Klein, S., 2019. Progressing emergent constraints on future climate change. Nat. Clim. Chang. 9, 269–278. https://doi.org/10.1038/s41558-019-0436-6

Harvey, B.J., Cook, P., Shaffrey, L.C., Schiemann, R., 2020. The Response of the Northern Hemisphere Storm Tracks and Jet Streams to Climate Change in the CMIP3, CMIP5, and CMIP6 Climate Models. Journal of Geophysical Research: Atmospheres 125, e2020JD032701. https://doi.org/10.1029/2020JD032701

He, B., Yu, Y., Bao, Q., Lin, P., Liu, H., Li, J., Wang, L., Liu, Y., Wu, G., Chen, K., Guo, Y., Zhao, S., Zhang, X., Song, M., Xie, J., 2020. CAS FGOALS-f3-L model dataset

descriptions for CMIP6 DECK experiments. Atmospheric and Oceanic Science Letters 13, 582–588. https://doi.org/10.1080/16742834.2020.1778419

He, C., Wu, B., Zou, L., Zhou, T., 2017. Responses of the Summertime Subtropical Anticyclones to Global Warming. Journal of Climate 30, 6465–6479. https://doi.org/10.1175/JCLI-D-16-0529.1

Held, I.M., Guo, H., Adcroft, A., Dunne, J.P., Horowitz, L.W., Krasting, J., Shevliakova, E., Winton, M., Zhao, M., Bushuk, M., Wittenberg, A.T., Wyman, B., Xiang, B., Zhang, R., Anderson, W., Balaji, V., Donner, L., Dunne, K., Durachta, J., Gauthier, P.P.G., Ginoux, P., Golaz, J.-C., Griffies, S.M., Hallberg, R., Harris, L., Harrison, M., Hurlin, W., John, J., Lin, P., Lin, S.-J., Malyshev, S., Menzel, R., Milly, P.C.D., Ming, Y., Naik, V., Paynter, D., Paulot, F., Rammaswamy, V., Reichl, B., Robinson, T., Rosati, A., Seman, C., Silvers, L.G., Underwood, S., Zadeh, N., 2019. Structure and Performance of GFDL's CM4.0 Climate Model. Journal of Advances in Modeling Earth Systems 11, 3691–3727. https://doi.org/10.1029/2019MS001829

Hofstadter, R., Bidegain, M., 1997. Performance of general circulation models in southeastern South America. Climate Research - CLIMATE RES 9, 101–105. https://doi.org/10.3354/cr009101

Huth, R., 2000. A circulation classification scheme applicable in GCM studies. Theor Appl Climatol 67, 1–18. https://doi.org/10.1007/s007040070012

Kreienkamp, F., Lorenz, P., Geiger, T., 2020. Statistically Downscaled CMIP6 Projections Show Stronger Warming for Germany. Atmosphere 11, 1245. https://doi.org/10.3390/atmos11111245

Li, J.-L.F., Xu, K.-M., Jiang, J.H., Lee, W.-L., Wang, L.-C., Yu, J.-Y., Stephens, G., Fetzer, E., Wang, Y.-H., 2020. An Overview of CMIP5 and CMIP6 Simulated Cloud Ice, Radiation Fields, Surface Wind Stress, Sea Surface Temperatures, and Precipitation Over Tropical and Subtropical Oceans. Journal of Geophysical Research: Atmospheres 125, e2020JD032848. https://doi.org/10.1029/2020JD032848

Li, L., Yu, Y., Tang, Y., Lin, P., Xie, J., Song, M., Dong, L., Zhou, T., Liu, L., Wang, Lu, Pu, Y., Chen, X., Chen, L., Xie, Z., Liu, Hongbo, Zhang, L., Huang, X., Feng, T., Zheng, W., Xia, K., Liu, Hailong, Liu, J., Wang, Y., Wang, Longhuan, Jia, B., Xie, F., Wang, B., Zhao, S., Yu, Z., Zhao, B., Wei, J., 2020. The Flexible Global Ocean-Atmosphere-Land System Model Grid-Point Version 3 (FGOALS-g3): Description and Evaluation. Journal of Advances in Modeling Earth Systems 12, e2019MS002012. https://doi.org/10.1029/2019MS002012

Lynch, D. R., Gray, W. G. (1979). A wave equation model for finite element tidal computations. Computers & Fluids, 7(3), 207–228. https://doi.org/10.1016/0045-7930(79)90037-9

Massonnet, F., Ménégoz, M., Acosta, M., Yepes-Arbós, X., Exarchou, E., Doblas-Reyes, F.J., 2020. Replicability of the EC-Earth3 Earth system model under a change in computing environment. Geoscientific Model Development 13, 1165–1178. https://doi.org/10.5194/gmd-13-1165-2020

Mauritsen, T., Bader, J., Becker, T., Behrens, J., Bittner, M., Brokopf, R., Brovkin, V., Claussen, M., Crueger, T., Esch, M., Fast, I., Fiedler, S., Fläschner, D., Gayler, V., Giorgetta, M., Goll, D.S., Haak, H., Hagemann, S., Hedemann, C., Hohenegger, C., Ilyina, T., Jahns, T., Jimenéz-de-la-Cuesta, D., Jungclaus, J., Kleinen, T., Kloster, S., Kracher, D., Kinne, S., Kleberg, D., Lasslop, G., Kornblueh, L., Marotzke, J., Matei, D., Meraner, K., Mikolajewicz, U., Modali, K., Möbis, B., Müller, W.A., Nabel, J.E.M.S., Nam, C.C.W., Notz, D., Nyawira, S.-S., Paulsen, H., Peters, K., Pincus, R., Pohlmann, H., Pongratz, J., Popp, M., Raddatz, T.J., Rast, S., Redler, R., Reick, C.H., Rohrschneider, T., Schemann, V., Schmidt, H., Schnur, R., Schulzweida, U., Six, K.D., Stein, L., Stemmler, I., Stevens, B., Storch, J.-S. von, Tian, F., Voigt, A., Vrese, P., Wieners, K.-H., Wilkenskjeld, S., Winkler, A., Roeckner, E., 2019. Developments in the MPI-M Earth System Model version 1.2 (MPI-ESM1.2) and Its Response to Increasing CO2. Journal of Advances in Modeling Earth Systems 11, 998–1038. https://doi.org/10.1029/2018MS001400

Meehl, G.A., Boer, G.J., Covey, C., Latif, M., Stouffer, R.J., 1997. Intercomparison makes for a better climate model. Eos, Transactions American Geophysical Union 78, 445–451. https://doi.org/10.1029/97EO00276

Meehl, G.A., Covey, C., McAvaney, B., Latif, M., Stouffer, R.J., 2005. Overview of the Coupled Model Intercomparison Project. Bulletin of the American Meteorological Society 86, 89–93.

Melo, E. (2016). Maré meteorológica na costa brasileira. In *Tese de professor Titular* (Issue April). https://doi.org/10.13140/RG.2.2.25966.31040

Mignot, J., Bony, S., 2013. Presentation and analysis of the IPSL and CNRM climate models used in CMIP5. Clim Dyn 40, 2089–2089. https://doi.org/10.1007/s00382-013-1720-1

Müller, W.A., Jungclaus, J.H., Mauritsen, T., Baehr, J., Bittner, M., Budich, R., Bunzel, F., Esch, M., Ghosh, R., Haak, H., Ilyina, T., Kleine, T., Kornblueh, L., Li, H., Modali, K., Notz, D., Pohlmann, H., Roeckner, E., Stemmler, I., Tian, F., Marotzke, J., 2018. A

Higher-resolution Version of the Max Planck Institute Earth System Model (MPI-ESM1.2-HR). Journal of Advances in Modeling Earth Systems 10, 1383–1413. https://doi.org/10.1029/2017MS001217

Nobre, P., Siqueira, L.S.P., de Almeida, R.A.F., Malagutti, M., Giarolla, E., Castelão, G.P., Bottino, M.J., Kubota, P., Figueroa, S.N., Costa, M.C., Baptista, M., Irber, L., Marcondes, G.G., 2013. Climate Simulation and Change in the Brazilian Climate Model. J. Climate 26, 6716–6732. https://doi.org/10.1175/JCLI-D-12-00580.1

O'Neill, B.C., Tebaldi, C., Vuuren, D.P. van, Eyring, V., Friedlingstein, P., Hurtt, G., Knutti, R., Kriegler, E., Lamarque, J.-F., Lowe, J., Meehl, G.A., Moss, R., Riahi, K., Sanderson, B.M., 2016. The Scenario Model Intercomparison Project (ScenarioMIP) for CMIP6. Geoscientific Model Development 9, 3461–3482. https://doi.org/10.5194/gmd-9-3461-2016

Ortega, G., Arias, P.A., Villegas, J.C., Marquet, P.A., Nobre, P., 2021. Present-day and future climate over central and South America according to CMIP5/CMIP6 models. International Journal of Climatology 41, 6713–6735. https://doi.org/10.1002/joc.7221

Parise, C. K., Calliari, L. J., Krusche, N., 2009. Extreme storm surges in the south of Brazil: Atmospheric conditions and shore erosion. Brazilian Journal of Oceanography, 57(3), 175–188. https://doi.org/10.1590/s1679-87592009000300002

Pastor, M.A., Casado, M.J., 2012. Use of circulation types classifications to evaluate AR4 climate models over the Euro-Atlantic region. Clim Dyn 39, 2059–2077. https://doi.org/10.1007/s00382-012-1449-2

Perez, J., Mendez, F.J., Menendez, M., Losada, I.J., 2014b. ESTELA: a method for evaluating the source and travel time of the wave energy reaching a local area. Ocean Dynamics 64, 1181–1191. https://doi.org/10.1007/s10236-014-0740-7

Perez, J., Menendez, M., Camus, P., Mendez, F.J., Losada, I.J., 2015. Statistical multi-model climate projections of surface ocean waves in Europe. Ocean Modelling, Waves and coastal, regional and global processes 96, 161–170. https://doi.org/10.1016/j.ocemod.2015.06.001

Perez, J., Menendez, M., Mendez, F.J., Losada, I.J., 2014. Evaluating the performance of CMIP3 and CMIP5 global climate models over the north-east Atlantic region. Clim Dyn 43, 2663–2680. https://doi.org/10.1007/s00382-014-2078-8

Peterson, R.G., Stramma, L., 1991. Upper-level circulation in the South Atlantic Ocean. Progress in Oceanography 26, 1–73. https://doi.org/10.1016/0079-6611(91)90006-8

Reboita, M.S., Ambrizzi, T., Silva, B.A., Pinheiro, R.F., da Rocha, R.P., 2019. The South Atlantic Subtropical Anticyclone: Present and Future Climate. Front. Earth Sci. 7. https://doi.org/10.3389/feart.2019.00008

Reichler, T., Kim, J., 2008. How Well Do Coupled Models Simulate Today's Climate? Bull. Amer. Meteor. Soc. 89, 303–312. https://doi.org/10.1175/BAMS-89-3-303

Rueda, A., Camus, P., Tomás, A., Vitousek, S., Méndez, F.J., 2016. A multivariate extreme wave and storm surge climate emulator based on weather patterns. Ocean Modelling 104, 242–251. https://doi.org/10.1016/j.ocemod.2016.06.008

Saha, S., Moorthi, S., Pan, H.-L., Wu, X., Wang, Jiande, Nadiga, S., Tripp, P., Kistler, R., Woollen, J., Behringer, D., Liu, H., Stokes, D., Grumbine, R., Gayno, G., Wang, Jun, Hou, Y.-T., Chuang, H., Juang, H.-M.H., Sela, J., Iredell, M., Treadon, R., Kleist, D., Delst, P.V., Keyser, D., Derber, J., Ek, M., Meng, J., Wei, H., Yang, R., Lord, S., Dool, H. van den, Kumar, A., Wang, W., Long, C., Chelliah, M., Xue, Y., Huang, B., Schemm, J.-K., Ebisuzaki, W., Lin, R., Xie, P., Chen, M., Zhou, S., Higgins, W., Zou, C.-Z., Liu, Q., Chen, Y., Han, Y., Cucurull, L., Reynolds, R.W., Rutledge, G., Goldberg, M., 2010. The NCEP Climate Forecast System Reanalysis. Bulletin of the American Meteorological Society 91, 1015–1058. https://doi.org/10.1175/2010BAMS3001.1

Sakamoto, T.T., Komuro, Y., Nishimura, T., Ishii, M., Tatebe, H., Shiogama, H., Hasegawa, A., Toyoda, T., Mori, M., Suzuki, T., Imada, Y., Nozawa, T., Takata, K., Mochizuki, T., Ogochi, K., Emori, S., Hasumi, H., Kimoto, M., 2012. MIROC4h—A New High-Resolution Atmosphere-Ocean Coupled General Circulation Model. Journal of the Meteorological Society of Japan. Ser. II 90, 325–359. https://doi.org/10.2151/jmsj.2012-301

Schulzweida, U., 2019. CDO User Guide (Version 1.9.8) http://doi.org/10.5281/zenodo.3539275

Scoccimarro, E., Gualdi, S., Bellucci, A., Sanna, A., Fogli, P.G., Manzini, E., Vichi, M., Oddo, P., Navarra, A., 2011. Effects of Tropical Cyclones on Ocean Heat Transport in a High-Resolution Coupled General Circulation Model. Journal of Climate 24, 4368–4384. https://doi.org/10.1175/2011JCLI4104.1

Smith, G.A., Hemer, M., Greenslade, D., Trenham, C., Zieger, S., Durrant, T., 2021. Global wave hindcast with Australian and Pacific Island Focus: From past to present. Geoscience Data Journal 8, 24–33. https://doi.org/10.1002/gdj3.104

Song, Y.H., Chung, E.-S., Shahid, S., 2021. Spatiotemporal differences and uncertainties in projections of precipitation and temperature in South Korea from CMIP6 and CMIP5 general circulation models. International Journal of Climatology 41, 5899–5919. https://doi.org/10.1002/joc.7159

Sun, X., Cook, K.H., Vizy, E.K., 2017. The South Atlantic Subtropical High: Climatology and Interannual Variability. J. Climate 30, 3279–3296. https://doi.org/10.1175/JCLI-D-16-0705.1

Swart, N.C., Cole, J.N.S., Kharin, V.V., Lazare, M., Scinocca, J.F., Gillett, N.P., Anstey, J., Arora, V., Christian, J.R., Hanna, S., Jiao, Y., Lee, W.G., Majaess, F., Saenko, O.A., Seiler, C., Seinen, C., Shao, A., Sigmond, M., Solheim, L., von Salzen, K., Yang, D., Winter, B., 2019. The Canadian Earth System Model version 5 (CanESM5.0.3). Geoscientific Model Development 12, 4823–4873. https://doi.org/10.5194/gmd-12-4823-2019

Swart, N.C., Fyfe, J.C., 2012. Observed and simulated changes in the Southern Hemisphere surface westerly wind-stress. Geophysical Research Letters 39. https://doi.org/10.1029/2012GL052810

Tatebe, H., Ogura, T., Nitta, T., Komuro, Y., Ogochi, K., Takemura, T., Sudo, K., Sekiguchi, M., Abe, M., Saito, F., Chikira, M., Watanabe, S., Mori, M., Hirota, N., Kawatani, Y., Mochizuki, T., Yoshimura, K., Takata, K., O'ishi, R., Yamazaki, D., Suzuki, T., Kurogi, M., Kataoka, T., Watanabe, M., Kimoto, M., 2019. Description and basic evaluation of simulated mean state, internal variability, and climate sensitivity in MIROC6. Geoscientific Model Development 12, 2727–2765. https://doi.org/10.5194/gmd-12-2727-2019

Taylor, K.E., Stouffer, R.J., Meehl, G.A., 2012. An Overview of CMIP5 and the Experiment Design. Bull. Amer. Meteor. Soc. 93, 485–498. https://doi.org/10.1175/BAMS-D-11-00094.1

Tian, B., Dong, X., 2020. The Double-ITCZ Bias in CMIP3, CMIP5, and CMIP6 Models Based on Annual Mean Precipitation. Geophysical Research Letters 47, e2020GL087232. https://doi.org/10.1029/2020GL087232

Tokarska, K.B., Stolpe, M.B., Sippel, S., Fischer, E.M., Smith, C.J., Lehner, F., Knutti, R., 2020. Past warming trend constrains future warming in CMIP6 models. Science Advances 6, eaaz9549. https://doi.org/10.1126/sciadv.aaz9549

Touzé-Peiffer, L., Barberousse, A., Le Treut, H., 2020. The Coupled Model Intercomparison Project: History, uses, and structural effects on climate research. WIREs Climate Change 11, e648. https://doi.org/10.1002/wcc.648

van Vuuren, D.P., Edmonds, J., Kainuma, M., Riahi, K., Thomson, A., Hibbard, K., Hurtt, G.C., Kram, T., Krey, V., Lamarque, J.-F., Masui, T., Meinshausen, M., Nakicenovic, N., Smith, S.J., Rose, S.K., 2011. The representative concentration pathways: an overview. Climatic Change 109, 5. https://doi.org/10.1007/s10584-011-0148-z

Vera, C., Silvestri, G., Liebmann, B., González, P., 2006. Climate change scenarios for seasonal precipitation in South America from IPCC-AR4 models. Geophysical Research Letters 33. https://doi.org/10.1029/2006GL025759

Villamayor, J., Ambrizzi, T., Mohino, E., 2018. Influence of decadal sea surface temperature variability on northern Brazil rainfall in CMIP5 simulations. Clim Dyn 51, 563–579. https://doi.org/10.1007/s00382-017-3941-1

Voldoire, A., Sanchez-Gomez, E., Salas y Mélia, D., Decharme, B., Cassou, C., Sénési, S., Valcke, S., Beau, I., Alias, A., Chevallier, M., Déqué, M., Deshayes, J., Douville, H., Fernandez, E., Madec, G., Maisonnave, E., Moine, M.-P., Planton, S., Saint-Martin, D., Szopa, S., Tyteca, S., Alkama, R., Belamari, S., Braun, A., Coquart, L., Chauvin, F., 2013. The CNRM-CM5.1 global climate model: description and basic evaluation. Clim Dyn 40, 2091–2121. https://doi.org/10.1007/s00382-011-1259-y

Volodin, E.M., Dianskii, N.A., Gusev, A.V., 2010. Simulating present-day climate with the INMCM4.0 coupled model of the atmospheric and oceanic general circulations. Izv. Atmos. Ocean. Phys. 46, 414–431. https://doi.org/10.1134/S000143381004002X

Volodin, E.M., Mortikov, E.V., Kostrykin, S.V., Galin, V.Y., Lykossov, V.N., Gritsun, A.S., Diansky, N.A., Gusev, A.V., Iakovlev, N.G., Shestakova, A.A., Emelina, S.V., 2018. Simulation of the modern climate using the INM-CM48 climate model. Russian Journal of Numerical Analysis and Mathematical Modelling 33, 367–374. https://doi.org/10.1515/rnam-2018-0032

Volodin, E.M., Mortikov, E.V., Kostrykin, S.V., Galin, V.Ya., Lykosov, V.N., Gritsun, A.S., Diansky, N.A., Gusev, A.V., Yakovlev, N.G., 2017. Simulation of modern climate with the new version of the INM RAS climate model. Izv. Atmos. Ocean. Phys. 53, 142–155. https://doi.org/10.1134/S0001433817020128

Volodin, E.M., Mortikov, E.V., Kostrykin, S.V., Galin, V.Ya., Lykossov, V.N., Gritsun, A.S., Diansky, N.A., Gusev, A.V., Iakovlev, N.G., 2017. Simulation of the present-day

climate with the climate model INMCM5. Clim Dyn 49, 3715–3734. https://doi.org/10.1007/s00382-017-3539-7

Watanabe, M., Suzuki, T., O'ishi, R., Komuro, Y., Watanabe, S., Emori, S., Takemura, T., Chikira, M., Ogura, T., Sekiguchi, M., Takata, K., Yamazaki, D., Yokohata, T., Nozawa, T., Hasumi, H., Tatebe, H., Kimoto, M., 2010. Improved Climate Simulation by MIROC5: Mean States, Variability, and Climate Sensitivity. Journal of Climate 23, 6312–6335. https://doi.org/10.1175/2010JCLI3679.1

Watanabe, S., Hajima, T., Sudo, K., Nagashima, T., Takemura, T., Okajima, H., Nozawa, T., Kawase, H., Abe, M., Yokohata, T., Ise, T., Sato, H., Kato, E., Takata, K., Emori, S., Kawamiya, M., 2011. MIROC-ESM 2010: model description and basic results of CMIP5-20c3m experiments. Geosci. Model Dev. 4, 845–872. https://doi.org/10.5194/gmd-4-845-2011

Wyser, K., van Noije, T., Yang, S., von Hardenberg, J., O'Donnell, D., Döscher, R., 2020. On the increased climate sensitivity in the EC-Earth model from CMIP5 to CMIP6. Geoscientific Model Development 13, 3465–3474. https://doi.org/10.5194/gmd-13-3465-2020

Klaus Wyser, Erik Kjellström, Torben Koenigk, Helena Martins, Ralf Döscher, 2020. Warmer climate projections in EC-Earth3-Veg: the role of changes in the greenhouse gas concentrations from CMIP5 to CMIP6. Environ. Res. Lett. 15. https://doi.org/10.1088/1748-9326/ab81c2

Yin, L., Fu, R., Shevliakova, E., Dickinson, R.E., 2013. How well can CMIP5 simulate precipitation and its controlling processes over tropical South America? Clim Dyn 41, 3127–3143. https://doi.org/10.1007/s00382-012-1582-y

Yukimoto, S., Adachi, Y., Hosaka, M., Sakami, T., Yoshimura, H., Hirabara, M., Tanaka, T.Y., Shindo, E., Tsujino, H., Deushi, M., Mizuta, R., Yabu, S., Obata, A., Nakano, H., Koshiro, T., Ose, T., Kitoh, A., 2012. A New Global Climate Model of the Meteorological Research Institute: MRI-CGCM3 —Model Description and Basic Performance—. Journal of the Meteorological Society of Japan. Ser. II 90A, 23–64. https://doi.org/10.2151/jmsj.2012-A02

Yukimoto, S., Kawai, H., Koshiro, T., Oshima, N., Yoshida, K., Urakawa, S., Tsujino, H., Deushi, M., Tanaka, T., Hosaka, M., Yabu, S., Yoshimura, H., Shindo, E., Mizuta, R., Obata, A., Adachi, Y., Ishii, M., 2019. The Meteorological Research Institute Earth System Model Version 2.0, MRI-ESM2.0: Description and Basic Evaluation of the

Physical Component. Journal of the Meteorological Society of Japan. Ser. II 97, 931–965. https://doi.org/10.2151/jmsj.2019-051

Yukimoto, S., Kawai, H., Koshiro, T., Oshima, N., Yoshida, K., Urakawa, S., Tsujino, H., Deushi, M., Tanaka, T., Hosaka, M., Yabu, S., Yoshimura, H., Shindo, E., Mizuta, R., Obata, A., Adachi, Y., Ishii, M., 2019. The Meteorological Research Institute Earth System Model Version 2.0, MRI-ESM2.0: Description and Basic Evaluation of the Physical Component. Journal of the Meteorological Society of Japan. Ser. II 97, 931–965. https://doi.org/10.2151/jmsj.2019-051

Ziehn, T., Chamberlain, M.A., Law, R.M., Lenton, A., Bodman, R.W., Dix, M., Stevens, L., Wang, Y.-P., Srbinovsky, J., 2020. The Australian Earth System Model: ACCESS-ESM1.5. JSHESS 70, 193–214. https://doi.org/10.1071/ES19035